Computational Investigation of the Chemical Modification of Polystyrene through Fluorocarbon and Hydrocarbon Ion Beam Deposition

Wen-Dung Hsu, Inkook Jang, and Susan B. Sinnott*

Department of Materials Science and Engineering, University of Florida, Gainesville, Florida 32611-6400

Received November 19, 2005. Revised Manuscript Received December 12, 2005

Classical molecular dynamics (MD) simulations are used to study the effect of continuous hydrocarbon (HC) and fluorocarbon (FC) ion beam deposition on a polystyrene (PS) surface. Plasma processing is widely used to chemically modify surfaces and deposit thin films, and it is well-accepted that polyatomic ions and neutrals within low-energy plasmas have a significant effect on the surface chemistry. Here a comparison is made of the manner in which polyatomic FC ions and similarly structured HC ions react with PS and produce new structures. Specifically, the deposition of beams of $C_3H_5^+$, CH_3^+, $C_3F_5^+$, and CF_3^+ on PS surfaces at experimental fluences is considered. The simulations predict that the backbone chains are modified significantly more than the phenyl groups and that larger ions with lower velocities and larger collision cross sections modify the substrate to a shallower depth than smaller ions with higher velocities, even though all their incident kinetic energies are the same. Additionally, HC ions dissociate more readily than FC ions during deposition. Consequently, smaller HC ions are predicted to chemically modify the polystyrene to a greater extent than larger HC ions or FC ions.

Introduction

Plasma processing is widely used in industry to modify surfaces or to deposit functional thin films. For example, fluorocarbon (FC) plasmas are commonly used to grow fluorinated polymer films with high thermal and chemical resistance, high dielectric constants, and low friction coefficients.[1−4] Hydrocarbon (HC) plasmas are typically used to produce thin films with high hardness and particular electronic band gap characteristics.[5−7]

It is well-accepted that polyatomic ions and neutrals within low-energy plasmas have a significant effect on the surface chemistry induced by plasma. Mass-selected ion beam deposition isolates the effect of polyatomic ions and investigates their contributions to the chemical modification of the surface. In addition, computer simulations of mass-selected ion beam deposition provide important details about the chemical reactions that occur during this process that are both complementary to experimental data and difficult to obtain directly in the experiments.[8−12]

Here, classical molecular dynamics (MD) simulations are carried out to study the continuous deposition of FC ions ($C_3F_5^+$ and CF_3^+) and HC ions ($C_3H_5^+$ and CH_3^+) onto polystyrene (PS) surfaces at experimental fluences. The goal is to investigate the differences in the ways in which these polyatomic ion beams chemically modify the PS. Specifically, the chemical products that are produced, their penetration depths into the PS surface, their reaction with the PS backbone chains and phenyl groups, and the amount of overall cross-linking in the PS are determined. These results are analyzed with respect to the relative sizes of the ions and the strengths of their interatomic bonds.

Computational Details

The MD simulations numerically integrate Newton's equations of motion with a fourth-order Nordsieck predictor-corrector algorithm,[13] and the atoms in the system are allowed to evolve with time in response to the applied forces. The short-ranged atomic interactions are calculated using the second-generation reactive empirical bond order (REBO) potential for hydrocarbons[14] and fluorocarbons,[15] while the long-ranged atomic interactions are calculated using a Lennard-Jones (LJ) potential. The REBO and LJ potentials are connected smoothly by spline interpolation.[16]

* Author to whom correspondence should be addressed. E-mail: sinnott@mse.ufl.edu.

(1) Takahashi, K.; Itoh, A.; Nakamura, T.; Tachibana, K. *Thin Solid Films* **2000**, *374*, 303−310.
(2) Tanaka, K.; Inomata, T.; Kogoma, M. *Thin Solid Films* **2001**, *386*, 217−221.
(3) da Costa, M.; Freire, F. L.; Jacobsohn, L. G.; Franceschini, D.; Mariotto, G.; Baumvol, I. R. *J. Diam. Relat. Mater.* **2001**, *10*, 910−914.
(4) Wang, J. H.; Chen, J. J.; Timmons, R. B. *Chem. Mater.* **1996**, *8*, 2212−2214.
(5) von Keudell, A. *Thin Solid Films* **2002**, *402*, 1−37.
(6) Khan, R. U. A.; Anguita, J. V.; Silva, S. R. P. *J. Non-Cryst. Solids* **2000**, *276*, 201−205.
(7) Grill, A. *Diamond Relat. Mater.* **1999**, *8*, 428−434.
(8) Jang, I.; Ni, B.; Sinnott, S. B. *J. Vac. Sci. Technol., A* **2002**, *20*, 564−568.
(9) Jang, I.; Phillips, R.; Sinnott, S. B. *J. Appl. Phys.* **2002**, *92*, 3363−3367.
(10) Jang, I.; Sinnott, S. B. *Appl. Phys. Lett.* **2004**, *84*, 5118−5120.
(11) Akin, F. A.; Jang, I.; Schlossman, M. L.; Sinnott, S. B.; Zajac, G.; Fuoco, E. R.; Wijesundara, M. B. J.; Li, M.; Tikhonov, A.; Pingali, S. V.; Wroble, A. T.; Hanley, L. *J. Phys. Chem. B* **2004**, *108*, 9656−9664.
(12) Wijesundara, M. B. J.; Ji, Y.; Ni, B.; Sinnott, S. B.; Hanley, L. J. *Appl. Phys.* **2000**, *88*, 5004−5016.
(13) Allen, M. P.; Tildesley, D. J. *Computer Simulation of Liquids*; Oxford Science Publications: Oxford, 1986.
(14) Brenner, D. W.; Shenderova, O. A.; Harrison, J. A.; Stuart, S. J.; Ni, B.; Sinnott, S. B. *J. Phys.: Condens. Matter* **2002**, *14*, 783−802.
(15) Jang, I. K.; Sinnott, S. B. *J. Phys. Chem. B* **2004**, *108*, 18993−19001.

10.1021/cm052557p CCC: $33.50
Published on Web 01/24/2006

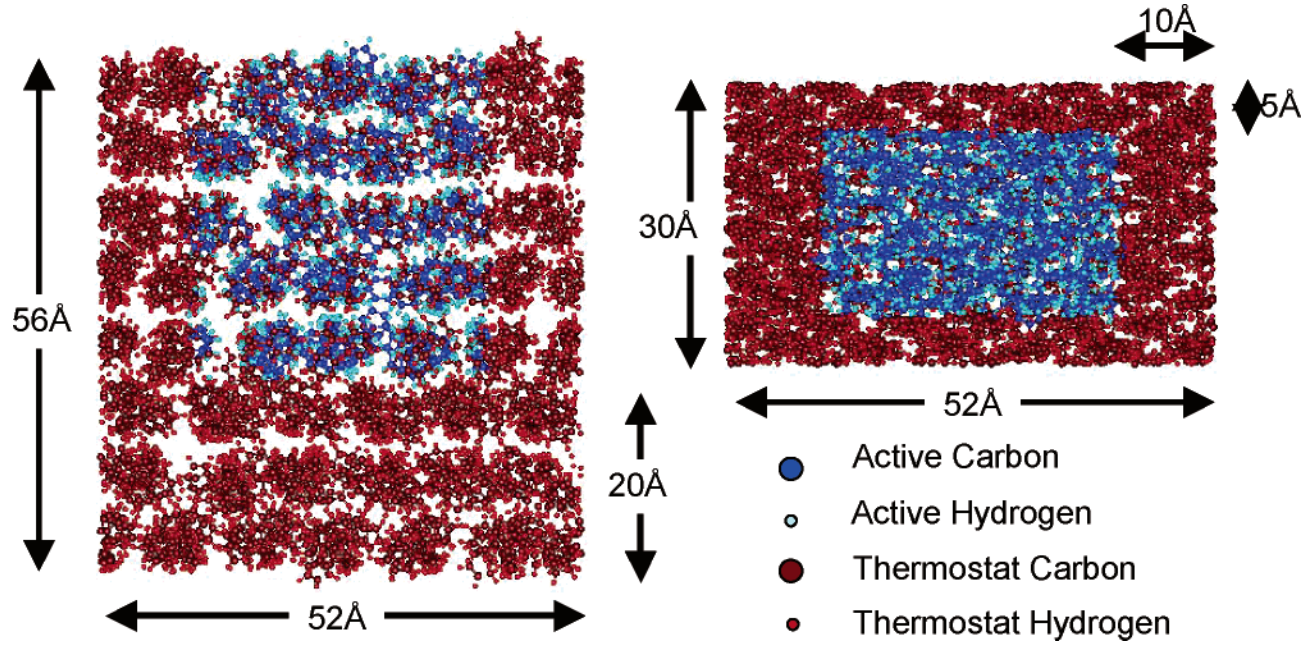

Figure 1. Snapshots of the side view (left) and top view (right) of the pristine PS surface after equilibration and prior to polyatomic ion beam deposition. The dark blue color represents carbon atoms in the active region, the light blue color represents hydrogen atoms in the active region, the dark red color represents carbon atoms in the thermostat region, and the light red color represents hydrogen atoms in the thermostat region.

Unlike molecular mechanics models, the REBO potential is able to predict new bond formation and bond breaking, both of which are crucial to accurately model the processes that occur in polyatomic ion beam deposition. Since it was developed, it has been successfully used to obtain insight into various processes that involve chemical reactions at surfaces, such as molecule−surface collisions,[17−22] cluster-beam surface deposition,[23,24] growth of diamond-like carbon films by hydrocarbon ion beams,[25,26] etching of Si surfaces by FC ion beams,[27−31] and the chemical vapor deposition of diamond.[32] However, because of the empirical and classical nature of the REBO potential, electronic effects, such as electronic excitations or true charging of the atoms, are not included. Therefore, ions with positive charges are treated as reactive radicals. Truly charged ions might be expected to react more aggressively than the simulated radicals. However, it is also true that many incident ions are rapidly neutralized as they approach the surface. These potentials are thus expected to provide qualitatively correct results and important insights into the chemical modification of polymers by mass-selected polyatomic ions.

A snapshot of the PS surface used in the MD simulations is shown in Figure 1. It is made up of eight layers of syndiotactic PS chains, with six chains per layer. These chains are aligned along the short side of the surface slab (which is 30 Å) such that 12 repeat units ($-CH_2-CHC_6H_5-$) fit within this length. The long side of the surface slab is 52 Å wide, the thickness normal to the surface is 56 Å, and the total number of atoms is approximately 10 000. Periodic boundary conditions[13] are applied within the surface plane to mimic an infinite surface. Every PS chain ends at the boundary to effectively wrap around on itself such that there are no surface slab edge effects.

To maintain the system temperature at 300 K during deposition, a thermostat is applied to some surface atoms. Specifically, the three bottom layers of the substrate and atoms within 5 Å from the two long sides of the slab, and 10 Å from the two short sides of the slab, have Langevin friction and stochastic forces applied to them.[13] This imitates the heat dissipation process of real substrate and prevents the surface from translating in response to polyatomic ion beam deposition. The rest of atoms are "active" and can evolve freely in response to the force fields formed by the surrounding atoms. Before deposition, the PS substrate is relaxed at 300 K for 3 ps at which point the system potential energy fluctuates by 0.0033 eV/atom around a constant value as a function of time.

Two beams of FC ions, one of $C_3F_5^+$ and one of CF_3^+, and two beams of HC ions, one of $C_3H_5^+$ and one of CH_3^+, are deposited on the active area of the PS substrate in separate simulation studies. Each beam contains a total of 240 $C_3F_5^+$ or $C_3H_5^+$ ions, or 400 CF_3^+ or CH_3^+ ions, such that the total F/H atom fluence is the same in all cases. Each ion in the continuously deposited beam impacts the PS surface at a randomly selected location within the active area and is randomly orientated relative to the surface. The total kinetic energy for each ion is 50 eV, and the incident angle is normal to the PS surface. The total fluence is equal to 1.8×10^{16} F/H atom/cm^2 and is comparable to experimental values.[12] The time interval between ion collisions with the surface is around 1.5 ps,

(16) Sinnott, S. B.; Shenderova, O. A.; White, C. T.; Brenner, D. W. *Carbon* **1998**, *36*, 1−9.
(17) Taylor, R. S.; Garrison, B. *J. Int. J. Mass Spectom. Ion Process.* **1995**, *143*, 225−233.
(18) Que, J. Z.; Radny, M. W.; Smith, P. V. *Phys. Rev. B* **1999**, *60*, 8686−8694.
(19) Ni, B.; Sinnott, S. B. *Phys. Rev. B* **2000**, *61*, R16343−R16346.
(20) Ni, B.; Andrews, R.; Jacques, D.; Qian, D.; Wijesundara, M. B. J.; Choi, Y. S.; Hanley, L.; Sinnott, S. B. *J. Phys. Chem. B* **2001**, *105*, 12719−12725.
(21) Mao, Z. G.; Sinnott, S. B. *J. Phys. Chem. B* **2000**, *104*, 4618−4624.
(22) Krantzman, K. D.; Postawa, Z.; Garrison, B. J.; Winograd, N.; Stuart, S. J.; Harrison, J. A. *Nucl. Instrum. Methods Phys. Res., Sect. B* **2001**, *180*, 159−163.
(23) Qi, L. F.; Sinnott, S. B. *J. Phys. Chem. B* **1997**, *101*, 6883−6890.
(24) Plaisted, T. A.; Ni, B.; Zahrt, J. D.; Sinnott, S. B. *Thin Solid Films* **2001**, *381*, 73−83.
(25) Neyts, E.; Bogaerts, A.; Gijbels, R.; Benedikta, J.; van de Sanden, M. C. M. *Nucl. Instrum. Methods Phys. Res., Sect. B* **2005**, *228*, 315−318.
(26) Neyts, E.; Bogaerts, A.; Gijbels, R.; Benedikt, J.; van de Sanden, M. C. M. *Diamond Relat. Mater.* **2004**, *13*, 1873−1881.
(27) Abrams, C. F.; Graves, D. B. *J. Appl. Phys.* **1999**, *86*, 5938−5948.
(28) Humbird, D.; Graves, D. B. *J. Appl. Phys.* **2004**, *96*, 791−798.
(29) Humbird, D.; Graves, D. B. *J. Appl. Phys.* **2004**, *96*, 65−70.
(30) Humbird, D.; Graves, D. B. *J. Appl. Phys.* **2004**, *96*, 2466−2471.
(31) Tanaka, J.; Abrams, C. F.; Graves, D. B. *J. Vac. Sci. Technol., A* **2000**, *18*, 938−945.
(32) Petukhov, A. V.; Fasolino, A. *Phys. Status Solidi A* **2000**, *181*, 109−114.

and after every five ions are deposited, the entire system is equilibrated for 3.4 ps to maintain the surface temperature at around 300 K. After the ion beam deposition process is complete, each system is further equilibrated for 25 ps at which point the system potential energy again fluctuates by 0.0033 eV/atom around a constant value with time. The FC ion beam deposition results are the same as those discussed by us previously[15] with additional analysis of the chemical modification of the PS surface to better facilitate a comparison with the new HC ion beam deposition results. The time step used in all the simulations is 0.20 fs.

Results and Discussion

There are no distinct, new fluorocarbon or hydrocarbon films formed as a result of polyatomic ion beam deposition over the time scales of these classical MD simulations. However, ion fragments and aggregates of fluorocarbons and hydrocarbons are generated that are consistent with experimentally[33−36] observed precursors to the growth of fluorocarbon or hydrocarbon thin films. For example, common experimentally observed precursor particles that are predicted to form in these simulations are small ion fragments, such as CF_2 and CH_2, and larger aggregates such as C_xF_y ($x > 2$, $y > 1$).[33−36] While the simulations predict that the $C_3H_5^+$ ion beam produces the largest number of aggregate chemical products (such as C_nH_m where $n > 3$ and $m > 5$), similar aggregates are formed for all the polyatomic ion beams considered here, with the CF_3^+ beam producing the smallest aggregates (C_2F_m, $m > 1$).

Figure 2 shows the final structures of the PS surfaces after the deposition of each of the four polyatomic ion beams. In all cases, the PS surfaces swell as a result of the deposition process. However, the resulting structures are significantly different after the deposition of the various ions considered. In particular, in the case of $C_3H_5^+$ ion beam deposition, chemical products form on and within the PS nearest the topmost surface layers. In contrast, in the case of the deposition of CH_3^+ ions, the chemical products are more evenly distributed throughout the PS. For the case of $C_3F_5^+$ and CF_3^+ deposition, the penetration profiles of ions and their fragments are similar to each other because CF_3^+ ions are more reactive with the surface than $C_3F_5^+$.

The simulations further indicate that the mechanism by which the surface swells depends on whether the incident ions are FCs or HCs. For example, CF_3^+ ion beam deposition causes much more surface swelling than $C_3F_5^+$ ion beam deposition because the smaller ion has a larger incident velocity (corresponding to the same incident kinetic energy of 50 eV/ion) and, thus, is able to transfer more kinetic energy to the local impact point on the PS surface. This kinetic energy leads to disruption of the PS ordering and causes the distances between the PS chains to increase. The $C_3F_5^+$ ion has a larger size and mass and, therefore, a lower incident velocity. Consequently, it transfers less kinetic energy to the impact point and leads to less swelling of the PS surface. On the other hand, both $C_3H_5^+$ and CH_3^+ ion beam depositions result in substantial surface swelling. The mechanism by which the CH_3^+ causes swelling is comparable to the mechanism by which the CF_3^+ ion does so. However, unlike $C_3F_5^+$, most of the $C_3H_5^+$ ions accumulate near the top of the PS surface rather than penetrating into the PS, thus effectively building up the surface.

The depth profiles of incident C, H, and F atomic densities in the PS after each deposition process is complete are illustrated in Figure 3. The figure indicates how the overall density of HC products is larger than the overall density of FC products. In other words, the HC ions, or their fragments or products, are most likely to remain in the PS and either form chemical bonds with the polymer chains or simply remain embedded in the PS surface over the time scales of these simulations. In contrast, the FC ions, or their fragments or products, are more likely to scatter away from the PS surface following deposition. The total density of deposited C atoms from the ions is therefore predicted to be higher in the case of HC polyatomic ion beam deposition than in the case of FC polyatomic ion beam deposition.

Figure 3 also reveals how the depth profiles of the products of the various ion beams differ from one anther. In most cases, the highest density of deposited atoms is at a depth of about 15 Å, and the distribution profile is a symmetric, bell-shaped curve. However, in the case of $C_3H_5^+$ ion beam deposition, most of the deposited atoms remain very near the top of the PS surface causing the depth profile distribution to be skewed and resemble half of a bell-shaped curve. This result is consistent with the data shown in Figure 2 and discussed above.

Figure 4 illustrates the chemical products (including ions and ion fragments) formed after ion beam deposition. The most plentiful product formed as a result of $C_3F_5^+$ ion beam deposition is C_3F_5, and the most plentiful products formed as a result of CF_3^+ ion beam deposition are CF_3 and CF_2. These results are explained by the strong carbon−fluorine interatomic bonds in the FC ions. The predictions for the HC ions are quite different. In particular, the most plentiful products (about 33% of the total products) formed as a result of $C_3H_5^+$ ion beam deposition are C_nH_m molecules, where $38 > n > 3$ and $49 > m > 5$ (these numbers only include atoms from incident ions, although some C_nH_m products bond to the PS chains), and the most plentiful products formed as a result of CH_3^+ ion beam deposition are CH, CH_2, and C_2H_n, where $n > 1$. Thus, the HC ions dissociate or react with other atoms more readily than the FC ions, and the most plentiful products from the larger ions are themselves larger than the most plentiful products from the smaller ions.

Another trend indicated in Figure 4 is that a higher fraction of the products formed as a result of HC ion beam deposition form chemical bonds with the PS chains on the time scales of these simulations than in the case of FC ion beam deposition. In particular, 50.5% of all of the chemical products form bonds with the PS substrate as a result of $C_3H_5^+$ ion beam deposition, and 65.4% of all of the chemical products form bonds with the PS substrate as a result of CH_3^+ ion beam deposition. In contrast, only 19.7% of all the chemical products form bonds with the PS substrate as a

(33) Fujita, K.; Ito, M.; Hori, M.; Goto, T. *Jpn. J. Appl. Phys., Part 1* **2003**, *42*, 650−656.
(34) Meier, M.; von Keudell, A. *J. Chem. Phys.* **2002**, *116*, 5125−5136.
(35) von Keudell, A.; Jacob, W. *Prog. Surf. Sci.* **2004**, *76*, 21−54.
(36) Schwarz-Selinger, T.; von Keudell, A.; Jacob, W. *J. Appl. Phys.* **1999**, *86*, 3988−3996.

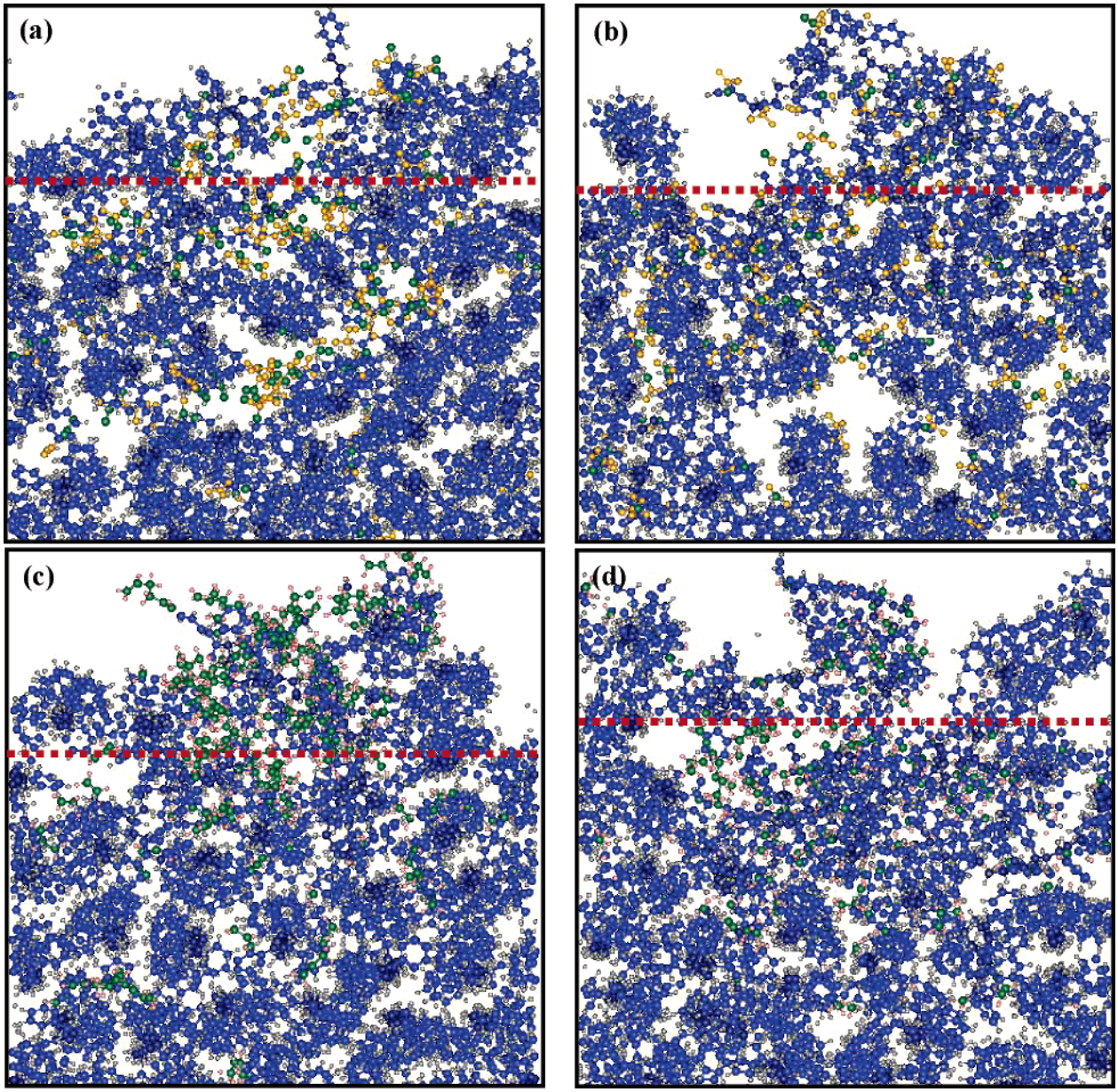

Figure 2. Snapshots of the PS surface after deposition and equilibration. (a) PS surface after $C_3F_5^+$ ion beam deposition. (b) PS surface after CF_3^+ ion beam deposition. (c) PS substrate surface after $C_3H_5^+$ ion beam deposition. (d) PS surface after CH_3^+ ion beam deposition. In a and b, the orange color represents F atoms from incident ions, the green color represents C atoms from incident ions, the gray color represents H atoms from PS surface, and the blue and dark blue represent C atoms from the phenyl C atoms and backbone C atoms, respectively, in the PS surface. In c and d, the pink color represents H atoms from incident ions and all other colors represent the same atom types as in a and b. The dotted red line represents the location of the top of the PS surface prior to ion beam deposition.

result of $C_3F_5^+$ ion beam deposition, and 25.0% of all of the chemical products form bonds with the PS substrate as a result of CF_3^+ ion beam deposition.

The quantitative results for $C_3H_5^+$ deposition differs from the results of our previous study,[8] which considered the deposition of many individual $C_3H_5^+$ ions on pristine PS surfaces. That study predicted that the major (about 30% of the total) chemical product is C_3H_5, that 50% of the C_3H_5 products form chemical bonds with the PS, and that 90% of the second most commonly formed species, CH_2, form chemical bonds with the PS.[8] These differences are because the previous study considered a statistical analysis of many individual $C_3H_5^+$ ions deposited onto a pristine PS surface rather than the continuous deposition of ions onto the same PS surface. As a result, there were no opportunities for the accumulation of damage or for the chemical products of multiple ion deposition events to interact with one another. In contrast, in this study, it is possible, for example, for the deposited $C_3H_5^+$ ions to form bonds with CH_2 products on the substrate and thus grow larger species.

While all the polyatomic ions have the same incident kinetic energy of 50 eV, they have different masses and velocities. The simulations indicate how the ions' masses and velocities influence the results of the deposition process. Specifically, they show that the ions with higher velocities cause more damage to the PS surface. Furthermore, the ions' mass and overall size affects their collision cross section with the surface. This too influences the transfer of energy to the PS and penetration into the surface. Figure 5 illustrates the predicted penetration depths for the various chemical products formed by the various ions (zero penetration depth means that the products remain at the top of the PS surface).

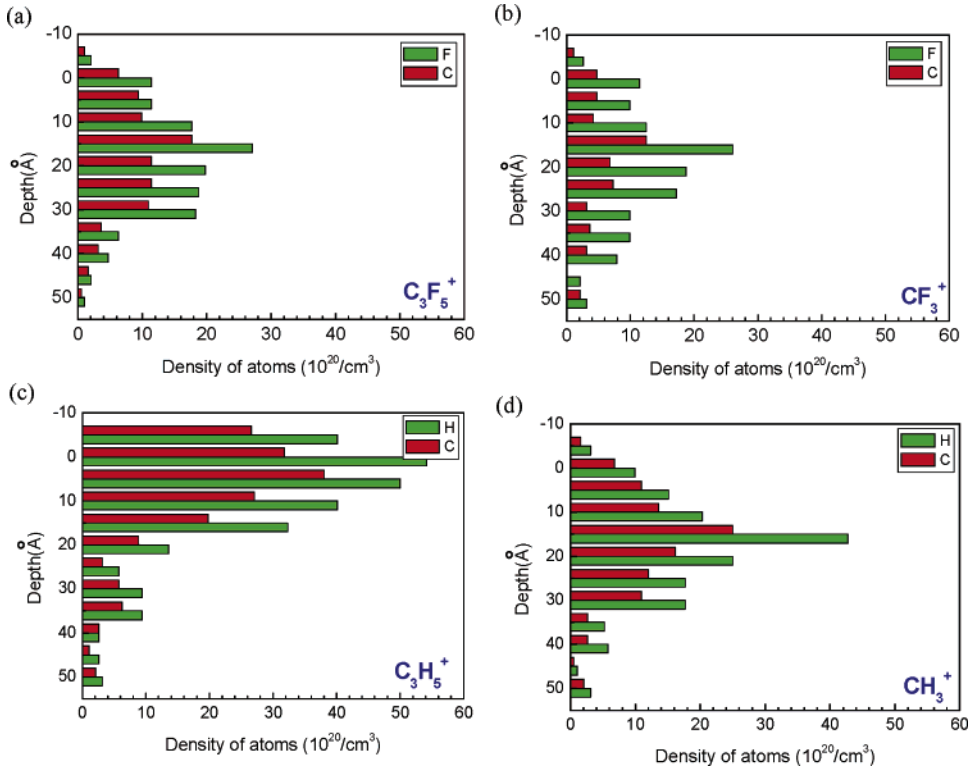

Figure 3. The depth profiles of carbon, hydrogen, and fluorine atom densities after ion beam deposition and equilibration. The carbon, hydrogen, and fluorine atoms counted here come from the incident ions only, and the hydrogen and fluorine atoms counted here are atoms that only bond with carbon atoms. (a) The depth profiles of carbon and fluorine atomic densities after $C_3F_5^+$ ion beam deposition. (b) The depth profiles of carbon and fluorine atomic densities after CF_3^+ ion beam deposition. (c) The depth profiles of carbon and hydrogen atomic densities after $C_3H_5^+$ ion beam deposition. (d) The depth profiles of carbon and hydrogen atomic densities after CH_3^+ ion beam deposition. Negative depths represent swelling of the surface.

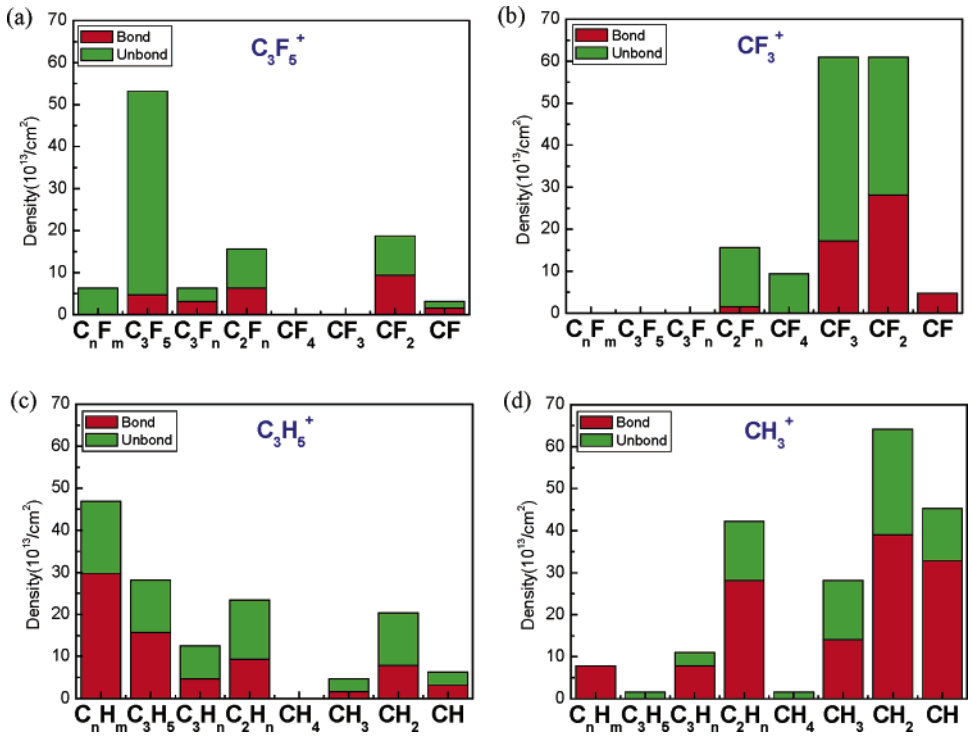

Figure 4. The densities of the various chemical products formed from the polyatomic ions after deposition and equilibration. The figure shows the density of chemical products formed after (a) $C_3F_5^+$, (b) CF_3^+, (c) $C_3H_5^+$, and (d) CH_3^+ ion beam deposition.

In general, the products that form chemical bonds most readily with the PS have shallower penetration depths. In the case of $C_3H_5^+$ ions, their fragment and resulting products show shallower penetration depths than $C_3F_5^+$ ions and their products. This is because once the products bond with the PS, they are trapped by the bonding and cannot go any deeper. However, in the case of CH_3^+ ion beam deposition, the ions' high velocity and small mass cause them to penetrate deeply into the PS until their kinetic energy is dissipated enough that they are able to form stable bonds.

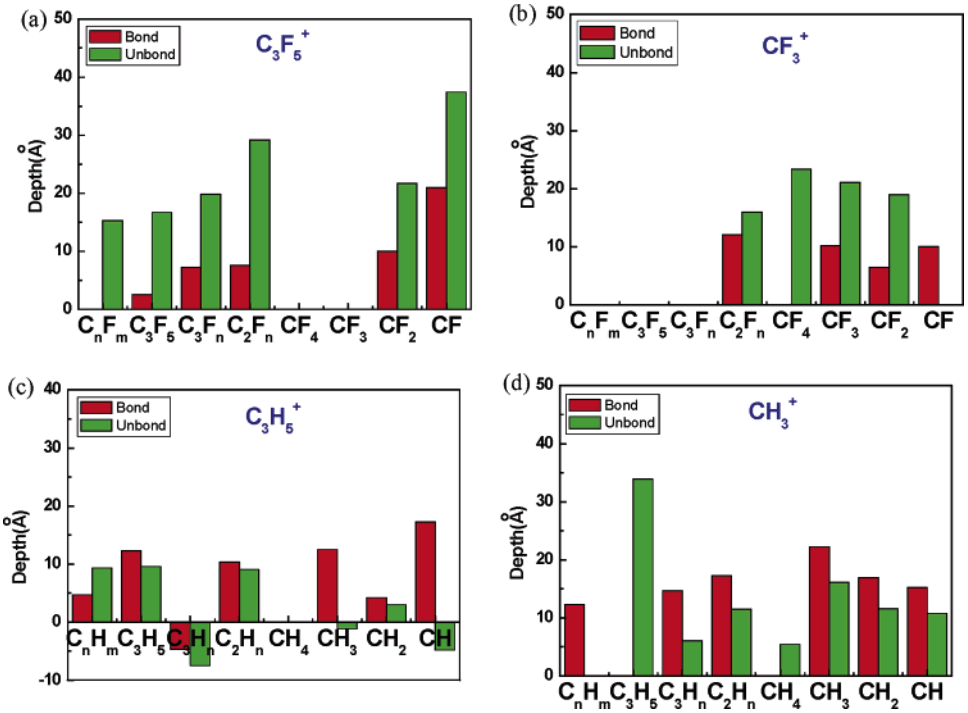

Figure 5. The penetration depths of the various chemical products formed after (a) $C_3F_5^+$, (b) CF_3^+, (c) $C_3H_5^+$, and (d) CH_3^+ ion beam deposition. Negative depths represent swelling of the surface.

Thus, a large fraction of the resulting products form covalent bonds to the PS chains and do so at a significant penetration depth.

Examination and comparison of Figures 4 and 5 also reveals where the majority of the chemical products formed remain in the PS substrate. For example, in the case of $C_3F_5^+$ ion deposition, the majority product, C_3F_5, bonds with the PS about 9 Å from the top of the PS surface. In the case of CF_3^+ ion deposition, the majority products, CF_3 and CF_2, also form bonds with the PS chains around 10 Å from the top of the PS surface. This suggests that the FC ions effectively fluorinate the PS. In the case of $C_3H_5^+$ ion deposition, the majority product, C_nH_m, form bonds with the PS around 5 Å from the top of the PS surface. Some products, such as C_3H_m, form bonds above the initial PS surface line. This implies that $C_3H_5^+$ ion deposition is effective for growing HC thin films on the PS substrate. However, in the case of CH_3^+ ion deposition, the results are quite different. As a result of the fact that the CH_3^+ ion is the smallest ion and has the largest velocity, most of its modifications occur deeper than the other ions at 13 Å. This indicates that CH_3^+ ions are not as effective as the other ions considered here at concentrating their chemical modification near the topmost part of the PS surface.

The simulations further allow us to examine the details of the PS chain modification as a result of polyatomic ion beam deposition. Table 1 shows the percentage of intact PS backbone chains as a function of depth after deposition. In general, in the case of large ions, damage to the PS chains is shallower than in the case of small ions. This is because the larger ions collide with more atoms in the PS once they impact the surface. They also have lower velocities relative to the smaller ions. In other words, they have a shorter mean free path within the polymer, a larger scattering cross section,

Table 1. Percentage of Intact PS Chains as a Function of Depth Following the Deposition of the Indicated Polyatomic Ion Beams

depth (Å)	$C_3F_5^+$	CF_3^+	$C_3H_5^+$	CH_3^+
0−7	0%	25%	0%	0%
7−14	25%	25%	25%	0%
14−21	75%	25%	100%	25%
21−28	100%	100%	100%	0%
28−35	100%	100%	100%	100%

Table 2. Percentage of Intact Phenyl Rings as a Function of Depth Following the Deposition of the Indicated Polyatomic Ion Beams

depth (Å)	$C_3F_5^+$	CF_3^+	$C_3H_5^+$	CH_3^+
0−7	23%	27%	9%	5%
7−14	86%	36%	41%	5%
14−21	100%	60%	90%	20%
21−28	100%	100%	100%	32%
28−35	100%	100%	100%	50%

and a slower incident velocity, which allows them to be scattered easily. The predicted trend in degree of modification of PS backbone chains for the ions considered here is $CH_3^+ > CF_3^+ > C_3F_5^+ > C_3H_5^+$.

Table 2 shows the percentage of intact phenyl rings as a function of depth after deposition. The extent of modification of phenyl rings from strong to weak is $CH_3^+ > CF_3^+ > C_3F_5^+ > C_3H_5^+$, which is the same trend deduced from Table 1. However, compared to Table 1, the depth of modification of the phenyl rings is significantly shallower than in the case of the PS backbone chains in general. This result makes sense, as the carbon−carbon conjugate bond is stronger than the carbon−carbon single bond, so PS backbone chains are more easily modified, on average, than the carbon−carbon bonds in the phenyl rings.

This point is confirmed in Table 3, which shows the number of backbone carbon atoms and phenyl ring carbon atoms that have undergone chemical reactions with incident ions. At first glance, it appears that the phenyl ring carbon atoms are modified more than the backbone carbon atoms.

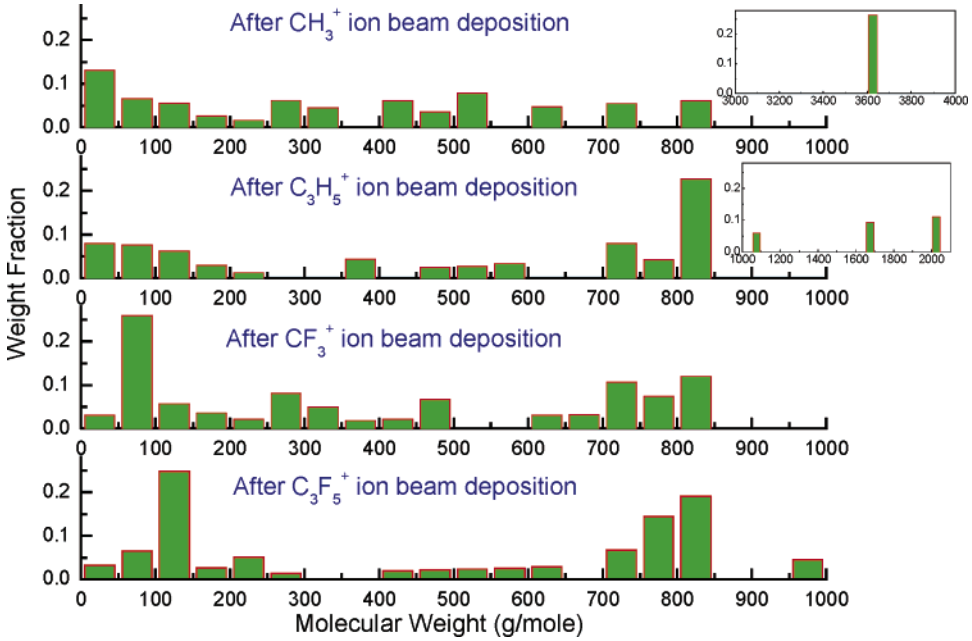

Figure 6. The distribution of molecular weights of chemical products in the PS after CH_3^+, $C_3H_5^+$, CF_3^+, and $C_3F_5^+$ ion beam deposition.

Table 3. The Number of Backbone Carbon Atoms and Phenyl Ring Carbon Atoms from the PS Surface that Have Undergone Chemical Reactions with the Incident Ions or Their Products

type of C atoms that have reacted	$C_3F_5^+$	CF_3^+	$C_3H_5^+$	CH_3^+
# of backbone C atoms	3	15	11	50
# of phenyl ring C atoms	16	46	53	134
# of phenyl ring C atoms/# of backbone C atoms	5.3	3.1	4.8	2.7

However, there are 2.8 times more phenyl ring carbon atoms than there are backbone carbon atoms prior to ion beam deposition. If we calculate the occupation volume of both kinds of carbon atoms in the substrate, the volume that the phenyl ring carbon atoms occupy is approximately 9.3 times larger than the volume occupied by backbone carbon atoms (as determined from a hard sphere model). This means phenyl carbon atoms are 9.3 times more likely to collide with an incoming ion or ion fragment than backbone carbon atoms. Therefore, if the modification strength is the same for phenyl ring carbon atoms and backbone carbon atoms, 9.3 times as many phenyl ring carbon atoms should react as backbone carbon atoms. However, column three in Table 3 indicates that the ratio of reacted phenyl ring carbon atoms to backbone carbon atoms ranges from 2.7 to 5.3. Thus, we may conclude that backbone carbon atoms are modified more readily than the phenyl ring carbon atoms.

The exact ratio of reacted phenyl ring carbon atoms to backbone carbon atoms also varies among the different incident ions. This indicates that the ability to modify the phenyl ring carbon atoms or the backbone carbon atoms depends to some extent on the properties of the ions. In particular, the ratio is about 5.3 for $C_3F_5^+$ deposition, 3.1 for CF_3^+ deposition, 4.8 for $C_3H_5^+$ deposition, and 2.7 for CH_3^+ deposition. The larger ions are better able to modify phenyl ring carbon atoms than small ions. This is especially true in the case of the $C_3F_5^+$, which is the heaviest ion considered here. It has a larger mass and its carbon−fluorine bonds are stronger than the carbon−hydrogen bonds in the HC ions, and thus it is more efficient at modifying phenyl rings than other kinds of incident ions. This is because it is able to transfer more of its kinetic energy to the phenyl ring through elastic collisions and chemical reactions, whereas the HC is more likely to bounce back or dissipate its kinetic energy by breaking apart. On the other hand, the CH_3^+ ions are less effective at modifying the phenyl rings but are quite effective at modifying the PS backbone chains.

After the ion beam deposition and equilibration processes are complete, the polymer chains or fragments that make up the modified PS surface, containing both original PS atoms and atoms from the incident ions, are analyzed and their molecular weights are calculated individually. Figure 6 illustrates the molecular weight distribution of chemical products in the PS formed after the polyatomic ion beam deposition processes are complete. Prior to deposition, the molecular weight of one PS chain within the active region of the PS surface (shown in blue in Figure 1) is 800−850 g/mole (within each periodic boundary condition cell). After deposition and equilibration, numerous small molecular weight chemical products are formed from the dissociation of ions and damage to the PS chains. If we look at the high molecular weight region (above 700 g/mole), which corresponds to only minor damage to the pristine PS chain, large incident ions, such as $C_3H_5^+$ and $C_3F_5^+$, produce more high molecular weight chemical products that remain in or on the PS surface than the small incident ions. This result is consistent with data shown in Tables 1 and 2.

Some large molecular weight species (more than twice as large as one pristine PS chain) are also formed after the HC ion beam deposition processes (see the insets in Figure 6). These chemical products are indicative of the greater cross-linking between PS chains and the greater degree of bonding of chemical products to the PS chains as a result of HC ion beam deposition compared to FC ion beam deposition.

Figure 7 displays the density of cross-linked points as a function of depth within the PS surface. Here, a cross-link

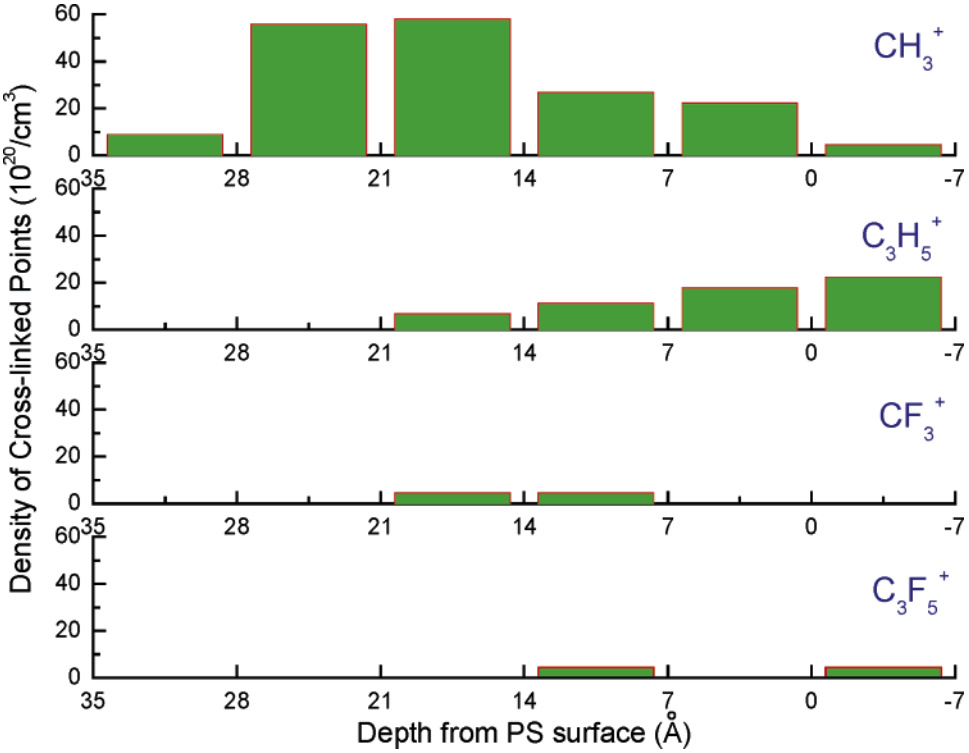

Figure 7. The density of cross-linked points as a function of depth in the PS surface after CH_3^+, $C_3H_5^+$, CF_3^+, and $C_3F_5^+$ ion beam deposition. The depth increment in the direction normal to the plane of the surface of 7 Å corresponds to approximately one layer of PS chains. The zero point is the original surface plane, and negative depths are indicative of PS surface swelling.

point is defined as a new chemical bond that is formed to PS backbone chains, PS backbone fragments, or PS phenyl ring fragments. The results indicate that, overall, HC ion beams produce higher PS cross-link densities than FC ion beams. Furthermore, comparison of $C_3H_5^+$ and CH_3^+ ion beam deposition processes indicates that $C_3H_5^+$ ion-produced cross-links are close to the top of the PS surface and extend outward from the original surface plane. Thus, these results predict that $C_3H_5^+$ ion beam deposition on PS surfaces will make these surfaces stronger and more brittle. The CH_3^+ ion-produced cross-links are located further away from the initial surface of the PS, around the fourth and fifth layers. In contrast, the FC ion beam deposition processes only generate slight cross-linking within the PS. However, the $C_3F_5^+$ ions also cross-link the PS on a shallower level than the CF_3^+ ions. In short, HC ions are much more efficient at cross-linking the PS than the FC, and in each case the larger ions produce more shallow cross-links, while the smaller ions produce deeper cross-links.

Conclusions

We have investigated the process of FC-ion and HC-ion beam deposition on PS surfaces and the way in which these polyatomic ion beams chemically modify the surface. The amount of resulting modification is influenced by the size of the ions, their velocities, and their intramolecular bond strengths. In particular, the size of the incident ions and their velocities affect the depth of the chemical modification within the PS, such that the larger the size of the ion, and the lower its velocity, the shallower the modification. In the case of the FC ions, the carbon−fluorine bond is strong, and so these ions are not easily broken apart during deposition. However, in the case of the HC ions, the carbon−hydrogen bond is not as strong, and so these ions are more readily broken into fragments on deposition. This causes the HC ions to more readily react with the PS surface than the comparable FC ions. The simulations predict that more than 50% of the chemical products produced in the HC ion beam deposition processes form chemical bonds with the PS, while less than 25% of the chemical products produced in the FC ion beam deposition processes form chemical bonds with the PS. The simulations furthermore provide details of how the PS surface is modified by the deposition of these ions and predict cross-link profiles for the various ion beams considered here.

This study thus provides a clear understanding of how differences between similarly structured FC and HC ions deposited in beams chemically modify PS surfaces. It also identifies likely mechanisms that are responsible for the observed outcomes.

Acknowledgment. We gratefully acknowledge the support of the National Science Foundation (Grant CHE-0200838).

CM052557P